

Chapter 7

Spots: Breathing, Drifting and Scattering in a Neural Field Model

Stephen Coombes, Helmut Schmidt, and Daniele Avitabile

Abstract Two dimensional neural field models with short range excitation and long range inhibition can exhibit localised solutions in the form of spots. Moreover, with the inclusion of a spike frequency adaptation current, these models can also support breathers and travelling spots. In this chapter we show how to analyse the properties of spots in a neural field model with linear spike frequency adaptation. For a Heaviside firing rate function we use an interface description to derive a set of four nonlinear ordinary differential equations to describe the width of a spot, and show how a stationary solution can undergo a Hopf instability leading to a branch of periodic solutions (breathers). For smooth firing rate functions we develop numerical codes for the evolution of the full space-time model and perform a numerical bifurcation analysis of radially symmetric solutions. An amplitude equation for analysing breathing behaviour in the vicinity of the bifurcation point is determined. The condition for a drift instability is also derived and a center manifold reduction is used to describe a slowly moving spot in the vicinity of this bifurcation. This analysis is extended to cover the case of two slowly moving spots, and establishes that these will reflect from each other in a head-on collision.

7.1 Introduction

Given the well known laminar structure of real cortical tissue it is natural to formulate neural field models in two spatial dimensions. For models with short range excitation and long range inhibition these have long been known to support localised solutions in the form of spots (commonly called bumps in one dimensional models). They are of particular interest to the neuroscience community since spatially localised bumps of activity have been linked to working memory (the

S. Coombes (✉) • H. Schmidt • D. Avitabile
School of Mathematical Sciences, University of Nottingham, Nottingham, NG7 2RD, UK.
e-mail: stephen.coombes@nottingham.ac.uk

temporary storage of information within the brain) in prefrontal cortex [17]. Perhaps not surprisingly their initial mathematical study was limited to solutions of one-dimensional models, and see [5, 12] for a review. With a further reduction in model complexity obtained by considering an effective single population model, obviating the need to distinguish between excitatory and inhibitory neuronal populations, Amari [1] showed for a Heaviside firing rate that bump solutions come in pairs, and that it is only the wider of the two that is stable. It was a surprisingly long time before Pinto and Ermentrout [24] demonstrated that a fuller treatment of inhibitory dynamics would allow a dynamic (Hopf) instability that could actually destabilise a wide bump. Blomquist et al. [3], further showed that this could lead to the formation of a stable breathing (spatially localised time periodic) solution. However, it is now known that inhibitory feedback is not the only way to generate dynamic instabilities of localised states, and a number of other physiological mechanisms are also possible. These include localised drive to the tissue [16], threshold accommodation (whereby the firing threshold is itself dynamic, mimicking a refractory mechanism) [6], synaptic depression [19], and spike frequency adaptation [8]. In comparison to their one dimensional counterparts, spots and their instabilities in two dimensions have received far less attention. Notable exceptions to this include the work of Laing and Troy [21] (focusing on numerical bifurcation analysis for smooth firing rates), Folias and Bressloff [15, 16] (focusing on localised drive), Owen et al. [23] (using an Evans function analysis to probe instabilities), and Coombes et al. [8] (using an interface approach). These last three pieces of work all focus on the Heaviside firing rate function.

In this chapter we develop new results for the description of spots in a two dimensional neural field model with spike frequency adaptation with both Heaviside and smooth firing rate choices. The techniques we develop are quite generic and may also be adapted to treat the other physiological mechanisms mentioned above for the generation of dynamic spot instabilities. We focus on a planar single population model that can be written as an integro-differential equation of the form

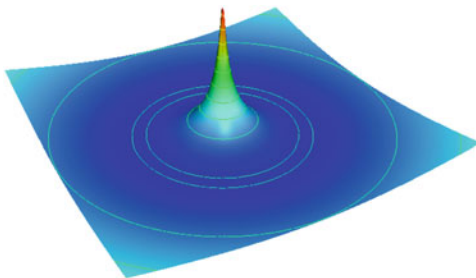
$$\frac{1}{\alpha} \frac{\partial u(\mathbf{r}, t)}{\partial t} = -u(\mathbf{r}, t) + \int_{\mathbb{R}^2} d\mathbf{r}' w(|\mathbf{r} - \mathbf{r}'|) f(u(\mathbf{r}', t)) - ga(\mathbf{r}, t), \quad (7.1)$$

$$\frac{\partial a(\mathbf{r}, t)}{\partial t} = -a(\mathbf{r}, t) + u(\mathbf{r}, t), \quad (7.2)$$

where $\mathbf{r} = (x_1, x_2) \in \mathbb{R}^2$ and $t \in \mathbb{R}^+$. Here the variable u represents synaptic activity and the kernel w represents anatomical connectivity. In real cortical tissues there are an abundance of metabolic processes whose combined effect is to modulate neuronal response. It is convenient to think of these processes in terms of local feedback mechanisms that modulate synaptic currents, described by the field a . Here, $g \in \mathbb{R}$ is the strength of the negative feedback. We shall take the firing rate to be a sigmoidal function, such as

$$f(u) = \frac{1}{1 + e^{-\beta(u-h)}}, \quad (7.3)$$

Fig. 7.1 A plot of the anatomical connectivity function describing short range excitation and long range inhibition. The form of $w(\mathbf{r})$, as expressed in (7.4), for $A_1 = 1 = \alpha_1$, $A_2 = -3/4$, and $\alpha_2 = 1/4$, generates a two dimensional wizard hat function



where $\beta > 0$ controls the steepness of the sigmoid around the threshold value h . Throughout the rest of this paper we shall work with the radially symmetric choice $w(\mathbf{r}) = w(r)$, with $r = |\mathbf{r}|$. To allow for some explicit calculations (though many of the results we develop do not require such a choice), we shall use the representation

$$w(r) = \sum_{i=1}^N A_i K_0(\alpha_i r), \quad A_i \in \mathbb{R}, \quad \alpha_i > 0, \quad (7.4)$$

where $K_\nu(x)$ is the modified Bessel function of the second kind, of order ν . For an appropriate combination of coefficients A_i and α_i this can generate an anatomical connectivity describing short range excitation and long range inhibition, with a wizard hat shape, as shown in Fig. 7.1.

In Sect. 7.2 we focus on a Heaviside firing rate and show how to extend the Amari interface approach to treat the spike frequency adaptation term. We develop a reduced description of a spot in terms of a set of four coupled nonlinear ordinary differential equations (ODEs). We solve these numerically, to find a narrow and wide branch of spot solutions that annihilate in a saddle-node bifurcation (with increasing threshold). The branch of wide spots is found to support a Hopf instability to a stable breathing solution. We move away from the Heaviside case in Sect. 7.3, and develop an equivalent partial differential equation (PDE) model that allows for straight-forward numerical implementation. We use this to probe radially symmetric solutions for models with sigmoidal firing rates, and not only confirm the results of our Heaviside analysis but show how results vary as one moves away from the limit of steep sigmoids. In Sect. 7.4 we develop an amplitude equation for analysing breathing behaviour (for a smooth firing rate function) in the vicinity of the bifurcation point. The condition for a drift instability, which describes the transition of a stationary spot to a (non-circular) travelling spot, is derived in Sect. 7.5. In Sect. 7.6 a center manifold reduction is used to describe a slowly moving spot in the vicinity of this bifurcation, and extended to cover the case of two slowly moving spots in Sect. 7.7. Interestingly the coupled ODE model for the spot pair can be analysed to show that these will reflect from each other in a head-on collision. Finally, in Sect. 7.8 we discuss natural extensions of the work in this Chapter.

7.2 Heaviside Firing Rate and Interface Dynamics

In the limit $\beta \rightarrow \infty$ the firing rate function (7.3) approximates a Heaviside function $H(u - h)$, and it is possible to explicitly construct localised states. Here we show how to extend the standard Amari interface approach to treat linear spike frequency adaptation. For simplicity we shall focus on radially symmetric solutions. A more general framework for describing the evolution of spreading interfaces that lack such a symmetry has recently been developed in [8]. We shall not pursue this here.

First let us rewrite the pair of Eqs. (7.1) and (7.2) in the form of a second order differential system:

$$u_{tt} + (1 + \alpha)u_t + \alpha(1 + g)u = \alpha(\psi + \psi_t), \quad (7.5)$$

where $\psi(\mathbf{r}, t) = \int_{\mathcal{B}(\mathbf{r}', t)} d\mathbf{r}' w(|\mathbf{r} - \mathbf{r}'|)$, and $\mathcal{B}(\mathbf{r}, t) = \{\mathbf{r}' | u(\mathbf{r}', t) \geq h\}$. For radially symmetric spot solutions of radius $R(t)$ that intersect the threshold exactly once (so that the active region is a single, simply connected region) we have that $(u(\mathbf{r}, t), \psi(\mathbf{r}, t)) = (u(r, t), \psi(r, t))$ with

$$\psi(r, t) = \int_0^{2\pi} d\theta \int_0^{R(t)} w\left(\sqrt{r^2 + r'^2 - 2rr' \cos \theta}\right) r' dr'. \quad (7.6)$$

Here $R(t)$ is defined by the level set condition $u(R(t), t) = h$. Differentiating this with respect to time gives an equation for the velocity of the spot interface in the form

$$\frac{dR}{dt} = - \left. \frac{\partial u(r, t)/\partial t}{\partial u(r, t)/\partial r} \right|_{r=R}, \quad (7.7)$$

Using (7.5) we may derive ODEs for $v = \partial u(r, t)/\partial t|_{r=R}$ and $z = \partial u(r, t)/\partial r|_{r=R}$ as

$$\frac{dv}{dt} + (1 + \alpha)v + \alpha(1 + g)h = \alpha [\psi + \psi_t]|_{r=R}, \quad (7.8)$$

$$\frac{d^2 z}{dt^2} + (1 + \alpha)\frac{dz}{dt} + \alpha(1 + g)z = \alpha \left. \frac{\partial}{\partial r} [\psi + \psi_t] \right|_{r=R}, \quad (7.9)$$

where we have assumed that R is slowly evolving so that $dz/dt = dR/dt z_R + z_t \approx z_t$. Hence, we may generate a system of four nonlinear ODEs for (R, v, z, y) to describe the evolution of the (radially symmetric) spot:

$$\frac{dR}{dt} = -\frac{v}{z}, \quad (7.10)$$

$$\frac{dv}{dt} = -(1 + \alpha)v - \alpha(1 + g)h + \alpha\Psi(R) - \alpha R v \Phi(R)/z, \quad (7.11)$$

$$\frac{dz}{dt} = y, \quad (7.12)$$

$$\frac{dy}{dt} = -(1 + \alpha)y - \alpha(1 + g)z + \alpha\Upsilon(R) - \alpha R^2 v \Omega(R)/z, \quad (7.13)$$

where

$$\Psi(R) = \int_0^{2\pi} d\theta \int_0^R w(\sqrt{R^2 + r^2 - 2Rr \cos \theta}) r dr, \quad (7.14)$$

$$\Phi(R) = \int_0^{2\pi} d\theta w(\mathcal{R}(\theta)), \quad \mathcal{R}(\theta) = R\sqrt{2(1 - \cos \theta)}, \quad (7.15)$$

$$\Upsilon(R) = \int_0^{2\pi} d\theta \int_0^R \frac{w'(\sqrt{R^2 + r^2 - 2Rr \cos \theta})}{\sqrt{R^2 + r^2 - 2Rr \cos \theta}} (R - r \cos \theta) r dr, \quad (7.16)$$

$$\Omega(R) = \int_0^{2\pi} d\theta \frac{w'(\mathcal{R}(\theta))}{\mathcal{R}(\theta)} (1 - \cos \theta). \quad (7.17)$$

For the anatomical connectivity function (7.4) then we have explicitly (using the summation properties of Bessel functions and Graf's formula) that

$$\Psi(R) = 2\pi \sum_{i=1}^N A_i \left\{ \frac{1}{\alpha_i^2} - \frac{R}{\alpha_i} K_1(\alpha_i R) I_0(\alpha_i R) \right\}, \quad (7.18)$$

$$\Phi(R) = 2\pi \sum_{i=1}^N A_i K_0(\alpha_i R) I_0(\alpha_i R), \quad (7.19)$$

$$\Upsilon(R) = \Psi'(R) - R\Phi(R) = -2\pi R \sum_{i=1}^N A_i K_1(\alpha_i R) I_1(\alpha_i R), \quad (7.20)$$

$$\Omega(R) = \Phi'(R)/(2R) = 2\pi \sum_{i=1}^N A_i \left\{ \frac{1}{2R^2} - \frac{\alpha_i}{R} K_1(\alpha_i R) I_0(\alpha_i R) \right\}. \quad (7.21)$$

Here $I_\nu(x)$ is the modified Bessel function of the first kind.

Steady states of (7.10)–(7.13) are given by $(R, v, z, y) = (R, 0, \Upsilon(R)/(1 + g), 0)$, where R is a solution of $\Psi(R) = (1 + g)h$. We can reconstruct the spatial profile of the stationary spot from knowledge of its radius by using $q(r) = \psi(r)/(1 + g)$, where $\psi(r)$ is given by (7.6) with $R(t) = R$. This can be explicitly calculated as

$$\psi(r) = 2\pi R \sum_{i=1}^N A_i L_i(r), \quad (7.22)$$

where

$$L_i(r) = \begin{cases} \frac{1}{\alpha_i} I_1(\alpha_i R) K_0(\alpha_i r) & r \geq R \\ \frac{1}{\alpha_i^2 R} - \frac{1}{\alpha_i} I_0(\alpha_i r) K_1(\alpha_i R) & r < R \end{cases}. \quad (7.23)$$

Here we restrict our attention to only those values of R that satisfy our original hypothesis, namely that the spot is a simply-connected active region.

The Jacobian of the system (7.10)–(7.13) around the steady state has one pair of eigenvalues given by

$$\lambda = \frac{-(1 + \alpha) \pm \sqrt{(1 - \alpha)^2 - 4\alpha g}}{2}, \quad (7.24)$$

and another pair that satisfy $\lambda^2 - \lambda J + K = 0$, where

$$J = -(1 + \alpha) - \alpha(1 + g)R \frac{\Phi(R)}{\Upsilon(R)}, \quad K = \alpha(1 + g) \frac{\Psi'(R)}{\Upsilon(R)}. \quad (7.25)$$

A Hopf bifurcation is possible when $J = 0$ and $K > 0$. Using (7.20) we see that this can happen when

$$R \frac{\Phi(R)}{\Upsilon(R)} = -\frac{(1 + \alpha)}{\alpha(1 + g)}, \quad \alpha g > 1. \quad (7.26)$$

which recovers a result in [8] obtained via a different method. The frequency of oscillation at the Hopf bifurcation is given by $\sqrt{\alpha g - 1}$.

The system of ODEs (7.10)–(7.13) is solved numerically with AUTO-07P [9] to generate the bifurcation diagram in Fig. 7.2 for a wizard hat function given by (7.4) with $N = 2$, $A_1 = (2\pi)^{-1}$, $A_2 = -(2\pi\gamma)^{-1}$, $\alpha_1 = 1$, $\alpha_2 = \mu$, with $\gamma, \mu > 0$. As expected we see a branch of wide spots and narrow spots that annihilate in a saddle-node bifurcation with increasing h . The inclusion of spike-frequency adaptation now allows for a pair of Hopf bifurcations on the wide branch of solutions, marked as HB_1 and HB_2 , determined by Eq. (7.26). Further numerical exploration shows that $\text{HB}_{1,2}$ give rise to a branch of periodic orbits, describing radially-symmetric breathers, whose period increases to infinity with decreasing h . This gives rise to homoclinic orbits, and we denote the associated homoclinic bifurcation points by $M_{1,2}$. Only the branch of breathers emanating from HB_2 is stable and it undergoes a sequence of period-doubling bifurcations in a small region of parameter space, as shown in the inset of Fig. 7.2, where h varies between 0.03609 and 0.03611.

In Fig. 7.3 we repeat the continuation for $\alpha = 1.25$. As expected, the branch of spots is the same as Fig. 7.2, but its stability properties change: the Hopf bifurcations $\text{HB}_{1,2}$ shift along the branch and are now connected in parameter space.

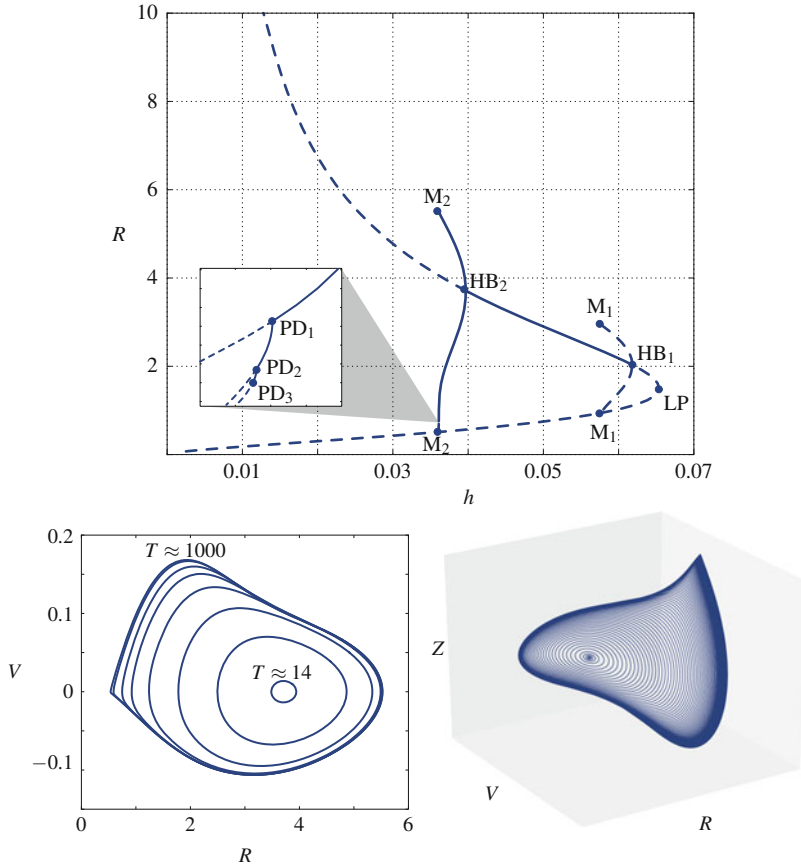


Fig. 7.2 Bifurcation diagram for spot solutions with a Heaviside firing rate function. *Solid (dashed) lines* are stable (unstable). Branches of periodic orbits originate from Hopf bifurcations of stationary spots. *Top*: branches of periodic solutions terminate at global homoclinic bifurcations M_1 and M_2 . Solutions emanating from HB_2 are initially stable and destabilise close to M_2 , where the branch undergoes a sequence of period-doubling bifurcations in a small region of parameter space (the *inset* shows h between 0.03609 and 0.03611). *Bottom*: stable periodic solutions between HB_2 and M_2 , with increasingly high periods, projected on the (V, R) -plane and the (V, R, Z) -space. Parameters are $\gamma = 4$, $\mu = 0.5$, $g = 1$, and $\alpha = 1.2$

Moreover, stable breathers emanating from HB_2 destabilise at a limit point rather than a global bifurcation. On the same plot, we show points along the branch where stationary spots become unstable with respect to azimuthal instabilities with D_m symmetry ($m = 2, \dots, 8$). Such critical points satisfy the equation (see [8] and also Chap. 3)

$$\frac{R}{|\Psi'(R)|} \int_0^{2\pi} d\theta \cos(m\theta) w(\mathcal{R}(\theta)) = \frac{\sum_{i=1}^N A_i K_m(\alpha_i R) I_m(\alpha_i R)}{\sum_{i=1}^N A_i K_1(\alpha_i R) I_1(\alpha_i R)} = 1, \quad (7.27)$$

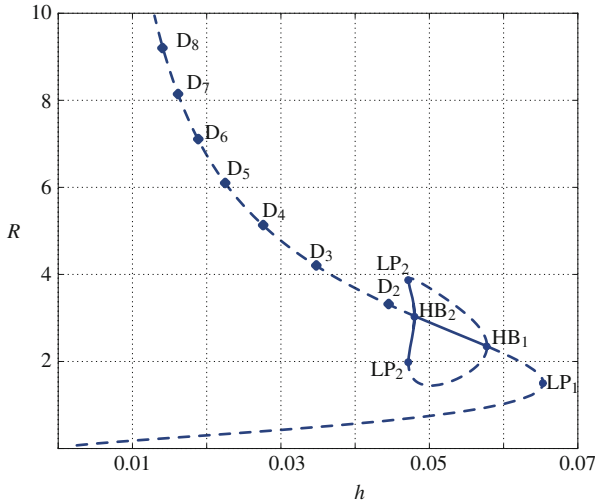


Fig. 7.3 Bifurcation diagram for spot solutions with a Heaviside firing rate function. Parameters as in Fig. 7.2 with the exception of α , which is set to 1.25. The branch of steady states coincides with the one in Fig. 7.2, as expected, but its stability depends on α : in this case HB_1 and HB_2 are connected in parameter space and stable breathers destabilise at a limit point. We also show points along the branch where spots become unstable to planar perturbations with D_2, \dots, D_8 symmetry

for $m = 2, 3, \dots$, where $\Psi(R)$ and $\mathcal{R}(\theta)$ are defined in (7.14) and (7.15). We point out that, following the branch for $\alpha = 1.25$ from bottom to top, the Hopf bifurcation HB_2 occurs before the D_2 instability, while the situation is reversed for $\alpha = 1.2$ (not shown). In Sect. 7.5 we further show that a solution with a drift instability, leading to a travelling spot, can occur as g increases through $1/\alpha$ (and note that the condition $\alpha g > 1$ is necessary for a breathing instability). A further weakly nonlinear analysis would be necessary to understand the competition between drifting and breathing at $g = 1/\alpha$.

The proximity of the limit point LP_1 to the Hopf bifurcation HB_1 (similarly to what was found for the case $\alpha = 1.2$ in Fig. 7.2, where we also have the global bifurcation M_1) suggests the possibility of a Bogdanov-Takens codimension 2 bifurcation. This scenario is present in a similar model (with localised drive) [15] and is confirmed by the two-parameter continuations plotted in Fig. 7.4.

7.3 Equivalent PDE Model and Numerical Bifurcation Analysis

In the previous section we derived a set of ODEs describing localised radially-symmetric solutions to (7.1) and (7.2), in the case when the firing rate f is a Heaviside function. It is interesting to compute similar solutions when f is a smooth

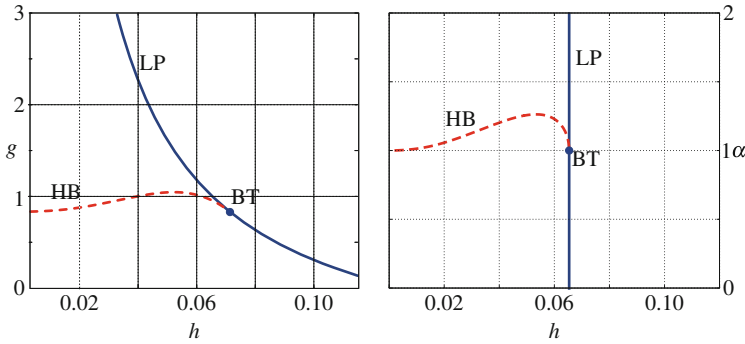


Fig. 7.4 Two-parameter continuations of the saddle-node bifurcation (*solid*), and Hopf bifurcations (*dashed*) of the stationary spots. Figure 7.2 corresponds to slices at $g = 1$ (in the *left panel*) and $\alpha = 1.2$ (in the *right panel*). Figure 7.3 corresponds to a slice $\alpha = 1.25$ (in the *right panel*). The curves meet at a Bogdanov-Takens bifurcation. Curves of homoclinic bifurcations $M_{1,2}$ are not shown

sigmoidal function, such as the one in (7.3). In this section, we follow ideas in [7, 13, 21] (and see also Chap. 5) that allow us to reformulate the nonlocal model defined by (7.1), (7.2), and (7.4), as a local model more suitable for direct numerical simulation and numerical continuation.

We begin by writing time-independent solutions of (7.1) and (7.2) as $(u(\mathbf{r}, t), a(\mathbf{r}, t)) = (q(\mathbf{r}), q(\mathbf{r}))$, where

$$q(\mathbf{r}) = \frac{1}{1 + g} \int_{\mathbb{R}^2} d\mathbf{r}' w(|\mathbf{r} - \mathbf{r}'|) f(q(\mathbf{r}')). \tag{7.28}$$

A spot is a radially-symmetric solution of (7.28) such that $q(\mathbf{r}) = q(r)$. We shall denote the (vector) spot solution by $S(r) = (q(r), q(r))$. Other localised solutions with dihedral symmetries of the regular polygon are also expected, and may arise via bifurcations of spots. This has been established for the case of a Heaviside firing rate [8], though we will not pursue this further here.

By re-arranging and taking a two dimensional Fourier transform of (7.28) we obtain

$$(1 + g)\hat{q}(k) = \hat{w}(k) \widehat{f \circ q}(k), \quad \hat{w}(k) = \sum_{i=1}^N \frac{2\pi A_i}{\alpha_i^2 + k^2}. \tag{7.29}$$

By taking the inverse Fourier transform of (7.29), we obtain a nonlinear PDE of the form

$$0 = -(1 + g)\mathcal{L}_1 q + \mathcal{L}_2 f(q), \tag{7.30}$$

where \mathcal{L}_1 and \mathcal{L}_2 are linear differential operators containing even spatial derivatives up to order $2N$ and $2N - 2$ respectively (using the result that the inverse Fourier transform of k^2 is $-\nabla^2$). The PDE formulation (7.30) is formally equivalent to (7.28).

In a similar way, it is possible to study the stability of stationary states with respect to radial perturbations. System (7.1) and (7.2) is written as a PDE

$$\begin{aligned}\mathcal{L}_1(\alpha^{-1}\partial_t u + u + ga) &= \mathcal{L}_2 f(u), \\ a_t &= u - a.\end{aligned}\tag{7.31}$$

Linear stability to radial perturbations can be inferred by posing $u(r, t) = q(r) + Q(r)e^{\lambda t}$, $a(r, t) = q(r) + A(r)e^{\lambda t}$ and linearising $\mathcal{L}_2 f(u)$ around $q(r)$, giving the generalised eigenvalue problem

$$\rho \mathcal{L}_1 Q = \mathcal{L}_2(f'(q)Q), \quad \rho = 1 + \frac{\lambda}{\alpha} + \frac{g}{1 + \lambda}.\tag{7.32}$$

We can then compute stationary solutions of system (7.1) and (7.2) and their spectra by prescribing suitable boundary conditions for (7.30) and (7.32) and discretising the operators \mathcal{L}_1 and \mathcal{L}_2 : for steady states, we use Newton's iterations to solve (7.30); a few eigenvalues are then computed (without inverting \mathcal{L}_1) applying Arnoldi iterations to (7.32). In passing, we note that it is also possible to study stability of radial solutions with respect to perturbations with dihedral symmetry, albeit this requires an amendment of the generalised eigenvalue problem (7.32).

Let us consider, for illustrative purposes, the wizard hat kernel used in Sect. 7.2 so that:

$$\mathcal{L}_1 = \Gamma_1 - \Gamma_2 \Delta_r + \Delta_r^2, \quad \mathcal{L}_2 = \Gamma_3 - \Gamma_4 \Delta_r,\tag{7.33}$$

where $\Delta_r = \partial_{rr} + r^{-1}\partial_r$ is the Laplacian operator expressed in radial coordinates and

$$\Gamma_1 = \mu^2, \quad \Gamma_2 = 1 + \mu^2, \quad \Gamma_3 = \mu^2 - \frac{1}{\gamma}, \quad \Gamma_4 = 1 - \frac{1}{\gamma}.\tag{7.34}$$

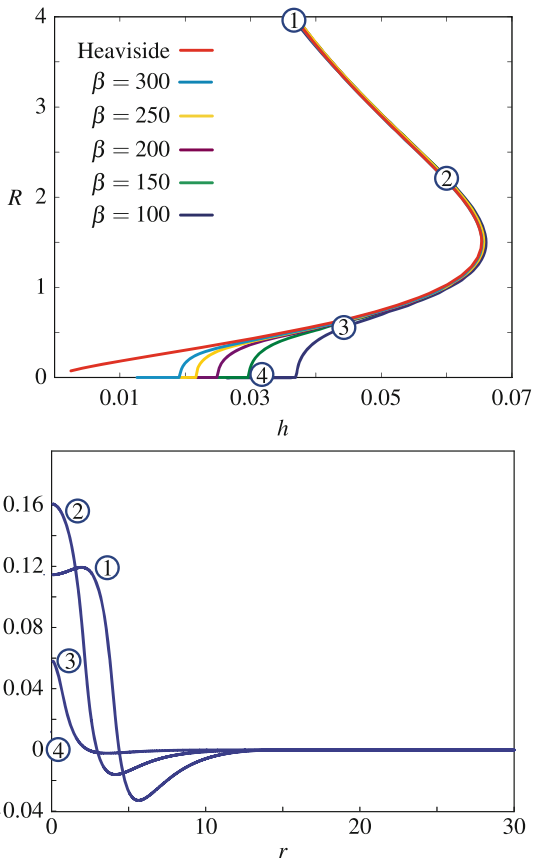
We then solve the nonlinear boundary-value problem

$$0 = -(1 + g)(\Gamma_1 - \Gamma_2 \Delta_r + \Delta_r^2)q + (\Gamma_3 - \Gamma_4 \Delta_r)f(q; h, \beta), \quad r \in (0, L)\tag{7.35}$$

$$0 = \partial_r q(0) = \partial_{rrr} q(0), \quad 0 = \partial_r q(L) = \partial_{rrr} q(L),\tag{7.36}$$

whose solutions can be continued in any of the control parameters μ , γ , h , β and g . We point out that, while equilibria of (7.1) and (7.2) do not depend upon α , this parameter influences their stability. The boundary-value problem (7.35) and (7.36) features no-flux boundary conditions at $r = L$, as in [20], but other choices are also possible: alternatively, one could pose $q(L) = \partial_{rr} q(L) = 0$.

Fig. 7.5 Localised spots found as solutions to the boundary-value problem (7.35). *Top:* branches of spots for various values of the sigmoidal firing-rate steepness, β ; on the vertical axis we plot a measure of the active region, that is, R is the largest number such that $q(R) = h$; the Heaviside branch is obtained by continuing equilibria of the system (7.10)–(7.13). *Bottom:* representative solutions along the branch $\beta = 100$. Control parameters: $\gamma = 4, \mu = 0.5, g = 1, L = 30$



We discretised (7.35) via second order centred finite differences with 3,200 grid points, on a domain with $L = 30$ and implemented a numerical continuation code written in MATLAB. Stability computations are performed using MATLAB’s in-built function `eigs`. In Fig. 7.5 we show a set of h -continuations for several values of the parameter β . These bifurcation diagrams are plotted in terms of the largest coordinate $R \in [0, L]$ for which $q(R) = h$; if $q(r) < h$ for all $r \in [0, L]$, as in pattern 4 of Fig. 7.5, we set $R = 0$. This allows us to compare steady states of (7.1) and (7.2), for increasingly high values of the sigmoidal firing rate steepness parameter β , with steady states of (7.10)–(7.13), which correspond to the Heaviside limit. Our numerical results show that the PDE formulation recovers the Heaviside case when $\beta \rightarrow \infty$, as confirmed also from the stability computations, contained in Fig. 7.6. Small-amplitude localised spots are unstable (bottom part of the branches) for our choice of control parameters, namely $\gamma = 4, \mu = 0.5, g = 1, L = 30$ and $\alpha = 1.2$. The branch features a saddle-node bifurcation and two Hopf bifurcations, which delimit a region of stable stationary spots. We also plot the spectra corresponding to the Hopf bifurcations, noting that the

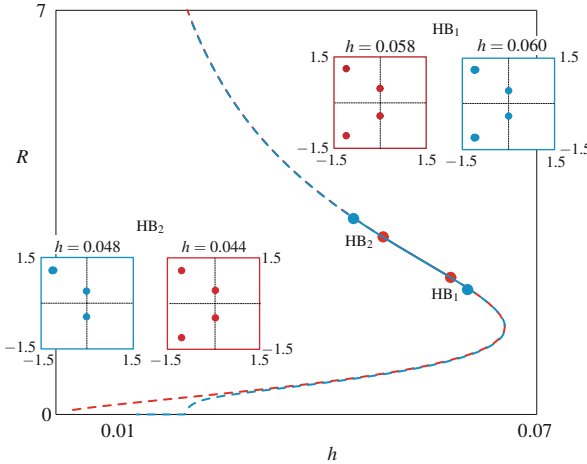


Fig. 7.6 Stability of radial spots for two solution branches of Fig. 7.5, namely Heaviside (red) and $\beta = 300$ (light blue). The bottom part of the branch is unstable and restabilises at a Hopf bifurcation (HB_1). The branch becomes unstable at a second Hopf bifurcation (HB_2). At the Hopf bifurcation points, we computed the corresponding eigenvalues for the Heaviside case (7.10)–(7.13) (red panels) and the first 10 eigenvalues obtained via (7.32) (light blue panels). Parameters: $\alpha = 1.25$, and other parameters as in Fig. 7.5

PDE formulation reproduces correctly the Hopf eigenvalues: other PDE eigenvalues (8, in the computations of Fig. 7.6) are clustered around the eigenvalues found using the interface approach (Heaviside firing rate) in Sect. 7.2. For steep sigmoids, the position of $HB_{1,2}$ changes slightly with respect to the Heaviside case.

Close to the HB_2 , we expect to find a branch of stable breathers, which can be found by direct numerical simulation of (7.31) with radially-symmetric operators (7.33). The time stepping is done without providing an explicit inverse of the operator \mathcal{L}_1 , but recasting (7.31) as

$$\begin{bmatrix} \alpha^{-1} \mathcal{L}_1 & 0 \\ 0 & 1 \end{bmatrix} \partial_t \begin{bmatrix} u \\ a \end{bmatrix} = \begin{bmatrix} -\mathcal{L}_1 & -g \mathcal{L}_1 \\ 1 & -1 \end{bmatrix} \begin{bmatrix} u \\ a \end{bmatrix} + \begin{bmatrix} \mathcal{L}_2 f(u) \\ 0 \end{bmatrix}, \quad (7.37)$$

discretising the left-hand side with a block-diagonal, sparse, time-independent mass matrix and then employing MATLAB’s `ode23s` solver with $RelTol=1e-3$ and $AbsTol=1e-6$. In the simulations of Fig. 7.7, we started from a stationary spot on the stable branch, decreased the value of h quasi-statically every 2,000 time units (corresponding to at least 100 oscillation cycles of the breathers) and found stable solutions with various amplitudes, spatial extensions and oscillation periods.

We notice that the breathers found with steep sigmoids have smaller amplitudes with respect to the ones found for the ODE model (7.10)–(7.13) (Fig. 7.3). Furthermore, the latter disappear at a limit point, while the former persist for much smaller values of the threshold h . This is to be expected as the ODE model is only valid under the assumption of a slowly varying R . In general we find that

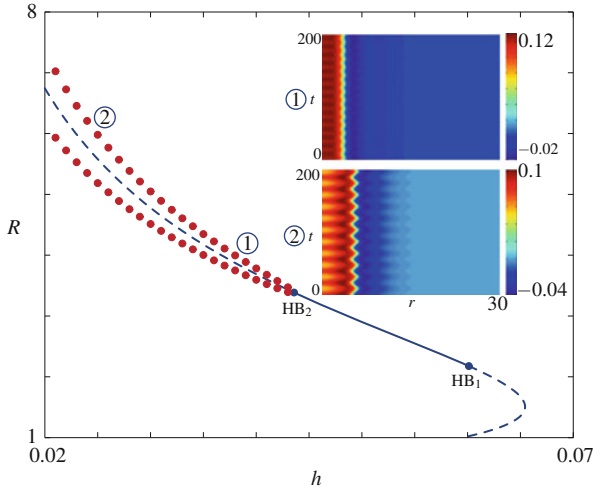


Fig. 7.7 Breathers originating from HB_2 for $\beta = 300$. Direct numerical simulations of (7.31) with radially-symmetric operators (7.33) show the existence of stable breathers, which are identified with the minimum and maximum of $R(t)$ during an oscillation period (*red dots*). As the threshold value h decreases, we find breathers with larger amplitudes, wider spatial extensions and longer periods. Numerical parameters as in Fig. 7.6

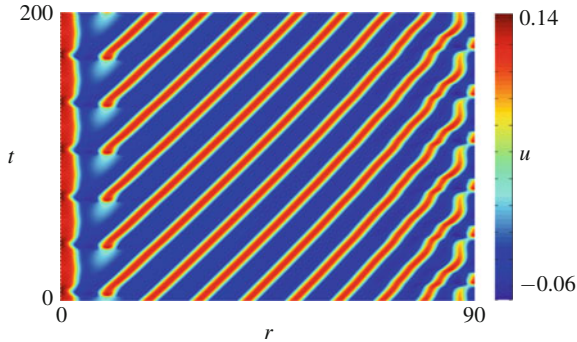


Fig. 7.8 Radial defect found by direct numerical simulation of system (7.31) with linear operators $\mathcal{L}_1, \mathcal{L}_2$ given by (7.33). This solution is found on a large domain, $L = 90$, for $h = 0.034$ and shallow sigmoidal firing rate, $\beta = 50$. Other parameters as in Fig. 7.6

the existence and stability of breathers depends sensitively on the steepness of the sigmoid: for instance, setting $\beta = 30$ and repeating the experiment of Fig. 7.7 leads to a trivial spatially-homogeneous equilibrium; on the other hand, increasing the sigmoid steepness to $\beta = 50$ leads to the formation of radial defects, that is, solutions in which a stable breather core emits periodically a travelling wave (see Fig. 7.8). Since our patterns are radially symmetric, these solutions correspond to a radial source emitting periodically travelling rings. Similar coherent structures were previously analysed in [25], continued in parameter space in [2] and their existence

was also reported in a nonlocal model with linear adaptation and localised stationary input by Folias and Bressloff [15].

7.4 Amplitude Equations for Breathing

Here we focus on a sigmoidal firing rate, such as given by (7.3), and show how to develop a description of the amplitude of a breathing solution just beyond the point of a breathing instability. We closely follow the ideas in [18], which were originally developed for the study of a three component reaction diffusion equation. A related analysis for one dimensional neural field models (and Heaviside firing rate function) can be found in [14] (and see also Chap. 4).

It is convenient to introduce the vector $X = (u, a)$ and the vector field \mathcal{F} , and write the model (7.1) and (7.2) in the form

$$X_t = \mathcal{F}(X; \sigma), \quad (7.38)$$

where σ represents a vector of system parameters, e.g. $\sigma = (\alpha, g, \beta, h)$, and

$$\mathcal{F}(X; \sigma) = MX + \alpha w \otimes F(X), \quad (7.39)$$

with

$$M = \begin{bmatrix} -\alpha & -\alpha g \\ 1 & -1 \end{bmatrix}, \quad F(X) = \begin{bmatrix} f(u) \\ 0 \end{bmatrix}. \quad (7.40)$$

Here the symbol \otimes denotes a two-dimensional spatial convolution.

Linearising about (7.28) gives

$$\partial_t V = \mathcal{L}V, \quad (7.41)$$

where

$$\mathcal{L} = M + \alpha w \otimes f'(q) \begin{bmatrix} 1 & 0 \\ 0 & 0 \end{bmatrix}. \quad (7.42)$$

For separable solutions of the form $V(\mathbf{r}, t) = \phi(\mathbf{r})e^{\lambda t}$, we generate an eigenvalue problem:

$$\mathcal{L}\phi = \lambda\phi. \quad (7.43)$$

Since the operator \mathcal{L} is in general not self-adjoint, then the eigenvalues, λ , and eigenfunctions, $\phi(\mathbf{r})$, may be complex. Because of translation and rotation invariance we expect the existence of an eigenvalue with $\lambda = 0$. The stationary spot is stable if all other eigenvalues have negative real part. For a breathing instability we are interested in the case that a pair of complex conjugate eigenvalues pass through

the imaginary axis under variation of some parameter, namely $\mathcal{L}\phi = \pm i\omega\phi$. Moreover, we shall focus on the case of radially symmetric breathing motions so that $\phi(\mathbf{r}) = \phi(r)$. We shall assume that a stationary spot S exists for a set of parameters $\sigma = \sigma_c$ for which $\mathcal{F}(S; \sigma_c) = 0$. We now introduce a small parameter $\eta \in \mathbb{R}$ and write $\sigma = \sigma_c + \eta(0, 0, 1, 0, \dots, 0)$, where the non-zero entry is associated to the system parameter that we wish to vary (and we only consider co-dimension 1 bifurcations here). In this case

$$X_t = \mathcal{F}(X; \sigma_c) + \eta\gamma(X), \quad (7.44)$$

where $\eta\gamma(X) = \mathcal{F}(X; \sigma_c + \eta) - \mathcal{F}(X; \sigma_c)$. For small η we expect to find a solution of the form

$$X(\mathbf{r}, t) = S(r) + A(t)e^{i\omega t}(\phi(r) + \eta\delta\phi(r)) + \text{cc} + \chi(\mathbf{r}, t), \quad (7.45)$$

where cc denotes the complex conjugate of the previous term. Here $A(t)$ is a slowly evolving amplitude ($A_t \sim \eta A$), $\eta\delta\phi$ is an unknown perturbation, and χ represents a decaying function in an orthogonal space to $\text{span}\{\phi\}$. Substituting into (7.44) and equating terms in $e^{i\omega t}$ gives an equation that relates A and $\delta\phi$:

$$\eta A (\mathcal{L} - i\omega) \delta\phi = \dot{A}\phi - \eta A \gamma' \phi - \frac{1}{2} A^2 \bar{A} \mathcal{F}''' \phi^2 \bar{\phi}. \quad (7.46)$$

Here the multiplication of vectors $\phi^2 \bar{\phi}$ is interpreted component wise, $\bar{\phi}$ denotes the complex conjugate of ϕ , γ' is the Fréchet derivative of γ with respect to X evaluated at $X = S$ and $\mathcal{F}^{(n)}$ is the n th Fréchet derivative of \mathcal{F} with respect to X evaluated at $X = S$:

$$\mathcal{F}^{(n)} = \alpha w \otimes \frac{d^n}{dq^n} f(q) \begin{bmatrix} 1 & 0 \\ 0 & 0 \end{bmatrix}. \quad (7.47)$$

According to the Fredholm alternative, Eq. (7.46) is solvable as long as the right hand side is orthogonal to the kernel of the operator $\mathcal{L} - i\omega$. It is now convenient to introduce the operator $\mathcal{L}^\dagger + i\omega$, where \mathcal{L}^\dagger is adjoint to, and has the same symmetry properties as \mathcal{L} . We shall denote the corresponding zero eigenfunction of $\mathcal{L}^\dagger + i\omega$ by ϕ^\dagger . We define the inner product of two vector functions a and b as

$$\langle a | b \rangle = \int_{\mathbb{R}^2} d\mathbf{r} \bar{a}(\mathbf{r}) \cdot b(\mathbf{r}), \quad (7.48)$$

where the dot \cdot denotes a vector dot product. Projecting (7.46) onto ϕ^\dagger and using the fact that $\langle \phi^\dagger | (\mathcal{L} - i\omega)\delta\phi \rangle = 0$ we obtain an equation for the evolution of the complex amplitude $A(t)$:

$$\dot{A} = A(M_1 |A|^2 + M_2 \eta), \quad (7.49)$$

where

$$M_1 = \frac{\langle \phi^\dagger | \mathcal{F}''' \phi^2 \bar{\phi} \rangle}{2\langle \phi^\dagger | \phi \rangle}, \quad M_2 = \frac{\langle \phi^\dagger | \gamma' \phi \rangle}{\langle \phi^\dagger | \phi \rangle}. \quad (7.50)$$

This analysis provides the basis for understanding the bifurcation diagrams obtained numerically in Sect. 7.3 and their criticality. Equation (7.49) has a trivial solution $A = 0$ describing a stationary spot, which for $\text{Re } M_2 < 0$ is a stable focus. If $\text{Re } M_2$ increase through zero the spot becomes unstable. For $\text{Re } M_2 > 0$ there is a non-trivial periodic solution $A(t) = R e^{i\Omega t}$, where

$$R = \sqrt{-\eta \frac{\text{Re } M_2}{\text{Re } M_1}}, \quad \Omega = \eta \text{Im } M_2 + R^2 \text{Im } M_1. \quad (7.51)$$

This non-trivial solution, describing a breather, is stable for $\text{Re } M_1 < 0$ (supercritical bifurcation) and unstable for $\text{Re } M_1 > 0$ (subcritical bifurcation). Considering a variation in the parameter g around some critical value g_c then

$$\gamma' = \left. \frac{\partial M}{\partial g} \right|_{g=g_c} = \begin{bmatrix} 0 & -\alpha \\ 0 & 0 \end{bmatrix}. \quad (7.52)$$

In the Appendix we show that ϕ^\dagger can be written in closed form as a linear transformation of ϕ :

$$\phi^\dagger = f'(q) \begin{bmatrix} 1/(\alpha g) & 0 \\ 0 & -1 \end{bmatrix} \bar{\phi}. \quad (7.53)$$

This means that we only have to numerically solve $\mathcal{L}\phi = i\omega\phi$ to compute the coefficients M_1 and M_2 in (7.49).

As well as a breathing bifurcation it is also possible for a stationary spot to undergo an instability to a travelling spot, via a drift instability. This has been recently studied for the case of a Heaviside firing rate [8]. Next we show how to analyse the case of a smooth firing rate.

7.5 Drifting

Here we adapt an argument in [23] to show how a spot can undergo an instability to a drifting pulse as g is increased through $1/\alpha$. From invariance of the full system (under rotation and translation) there exist Goldstone modes $\phi_i = \partial S(r)/\partial x_i$, $i = 1, 2$, such that

$$\mathcal{L}\phi_i = 0. \quad (7.54)$$

One of the possible destabilisations of the spot S occurs when one of the other modes exactly coincides with ϕ_i under parameter variation. Because of this parameter degeneracy a generalised eigenfunction ψ_i of \mathcal{L} appears:

$$\mathcal{L}\psi_i = -\phi_i. \quad (7.55)$$

The solvability condition for (7.55) leads to an equation defining the bifurcation point in the form

$$\langle \phi_i^\dagger | \phi_i \rangle = 0, \quad (7.56)$$

where ϕ_i^\dagger is the eigenfunction of the operator \mathcal{L}^\dagger with zero eigenvalue. More clearly we write $\mathcal{L}^\dagger \phi_i^\dagger = 0$ and $\mathcal{L}^\dagger \psi_i^\dagger = -\phi_i^\dagger$, normalised by $\langle \psi_i | \phi_j \rangle = \langle \psi_i | \psi_j^\dagger \rangle = 0$, and

$$\langle \phi_i | \psi_j^\dagger \rangle = \langle \psi_i | \phi_j^\dagger \rangle = \pi \delta_{i,j}. \quad (7.57)$$

Using (7.53) the inner product in Eq. (7.56) can be easily calculated, giving

$$0 = \left(\frac{1}{\alpha g} - 1 \right) \int_{\mathbb{R}^2} d\mathbf{r} f'(q(r)) \left(\frac{\partial q(r)}{\partial x_i} \right)^2. \quad (7.58)$$

Hence, a spot will lose stability as g increases through $1/\alpha$ and begin to drift (translate). Note that a model of synaptic depression can also destabilise a spot in favour of a travelling pulse [4].

7.6 Center Manifold Reduction: Particle Description

Here we adapt the technique in [11], originally developed to describe spot dynamics in multi-component reaction-diffusion equations, to derive a reduced description of a slowly moving spot. Beyond a drift instability, and for small η , we expect to find a solution of (7.44) that is a translating spot. In terms of a translation operator $\tau(\mathbf{p})u(\mathbf{r}, t) = u(\mathbf{r} - \mathbf{p}, t)$, $\mathbf{p} \in \mathbb{R}^2$ we may write this solution as

$$X(\mathbf{r}, t) = \tau(\mathbf{p}) \left[S(r) + \sum_{j=1}^2 a_j(t) \psi_j(\mathbf{r}) + \chi(\mathbf{r}, t) \right], \quad (7.59)$$

where \mathbf{p} denotes the location of the spot, $a_{1,2}$ are time dependent amplitudes, and χ is a function in an orthogonal space to $\text{span}\{\phi_i, \psi_i\}$. Differentiating X with respect to t gives

$$X_t = \tau(\mathbf{p}) \left[-\dot{\mathbf{p}} \cdot \nabla_{\mathbf{r}} X + \sum_{j=1}^2 \dot{a}_j \psi_j + \chi_t \right]. \quad (7.60)$$

Using (7.59) we may calculate the first term on the right hand side of (7.60) using

$$\dot{\mathbf{p}} \cdot \nabla_{\mathbf{r}} X = \dot{\mathbf{p}} \cdot \nabla_{\mathbf{r}} S(r) + a_1 \dot{\mathbf{p}} \cdot \nabla_{\mathbf{r}} \psi_1(\mathbf{r}) + a_2 \dot{\mathbf{p}} \cdot \nabla_{\mathbf{r}} \psi_2(\mathbf{r}) + \dot{\mathbf{p}} \cdot \nabla_{\mathbf{r}} \chi(\mathbf{r}, t). \quad (7.61)$$

The corresponding right hand side of (7.44) for the solution (7.59) can be expanded as

$$\tau(\mathbf{p}) \left\{ - \sum_{j=1}^2 a_j \phi_j + \mathcal{L} \chi + \frac{1}{2} \mathcal{F}'' W^2 + \frac{1}{6} \mathcal{F}''' W^3 + \eta \gamma(S(r)) + \eta \gamma'(S(r)) W + \dots \right\}, \quad (7.62)$$

where the N th power of the vector $W = \sum_j a_j \psi_j + \chi$ is interpreted component wise. Taking the inner product of both sides of (7.44) with ψ_i^\dagger gives

$$\begin{aligned} \langle X_t | \psi_1^\dagger \rangle &= -\dot{p}_1 \langle \phi_1 | \psi_1^\dagger \rangle, & (7.63) \\ \langle X_t | \psi_2^\dagger \rangle &= -\dot{p}_2 \langle \phi_2 | \psi_2^\dagger \rangle, \\ \langle \mathcal{F}(X; \sigma_c) + \eta \gamma(X) | \psi_1^\dagger \rangle &= -a_1 \langle \phi_1 | \psi_1^\dagger \rangle, \\ \langle \mathcal{F}(X; \sigma_c) + \eta \gamma(X) | \psi_2^\dagger \rangle &= -a_2 \langle \phi_2 | \psi_2^\dagger \rangle. \end{aligned}$$

Using (7.44) and equating expressions in (7.63) gives an equation for the evolution of the spot position as

$$\dot{\mathbf{p}} = \mathbf{a}. \quad (7.64)$$

Hence we may interpret \mathbf{a} as the spot velocity. To determine the dynamics for \mathbf{a} we write χ as a function that is quadratic in the amplitudes a_i and linear in η :

$$\chi = a_1^2 V_1(\mathbf{r}) + a_2^2 V_2(\mathbf{r}) + a_1 a_2 V_3(\mathbf{r}) + \eta V_4(\mathbf{r}). \quad (7.65)$$

Demanding that terms at this order balance requires

$$a_1 \mathbf{a} \cdot \nabla_{\mathbf{r}} \psi_1 + a_2 \mathbf{a} \cdot \nabla_{\mathbf{r}} \psi_2 = \mathcal{L} \chi + \frac{1}{2} \mathcal{F}'' (\mathbf{a} \cdot \psi)^2 + \eta \gamma(S), \quad \psi = (\psi_1, \psi_2). \quad (7.66)$$

Equating terms in $a_i a_j$ and η shows that

$$-\mathcal{L} V_1(\mathbf{r}) = \frac{1}{2} \mathcal{F}'' (\psi_1)^2 + \nabla_{x_1} \psi_1, \quad (7.67)$$

$$-\mathcal{L} V_2(\mathbf{r}) = \frac{1}{2} \mathcal{F}'' (\psi_2)^2 + \nabla_{x_2} \psi_2, \quad (7.68)$$

$$-\mathcal{L} V_3(\mathbf{r}) = \mathcal{F}'' \psi_1 \psi_2 + \nabla_{x_2} \psi_1 + \nabla_{x_1} \psi_2, \quad (7.69)$$

$$-\mathcal{L} V_4(\mathbf{r}) = \gamma(S(r)). \quad (7.70)$$

Here multiplication of vectors $\psi_i \psi_j$ is interpreted component wise. We now take the inner product of both sides of (7.44) with ϕ_i^\dagger :

$$\langle X_t | \phi_1^\dagger \rangle = -\dot{p}_1 \langle \chi_{x_1} | \phi_1^\dagger \rangle + \dot{a}_1 \langle \psi_1 | \phi_1^\dagger \rangle, \quad (7.71)$$

$$\langle X_t | \phi_2^\dagger \rangle = -\dot{p}_2 \langle \chi_{x_2} | \phi_2^\dagger \rangle + \dot{a}_2 \langle \psi_2 | \phi_2^\dagger \rangle, \quad (7.72)$$

$$\begin{aligned} \langle \mathcal{F}(X; \sigma_c) + \eta \gamma(X) | \phi_i^\dagger \rangle &= \langle \mathcal{L} \chi + \frac{1}{2} \mathcal{F}'' W^2 + \frac{1}{6} \mathcal{F}''' W^3 + \eta \gamma(S(r)) \\ &\quad + \eta \gamma'(S(r)) W | \phi_i^\dagger \rangle. \end{aligned} \quad (7.73)$$

Making use of (7.66) and working to only cubic order in the amplitudes so that $W^2 \approx (\mathbf{a} \cdot \psi)^2 + 2(\mathbf{a} \cdot \psi) \chi$ and $W^3 \approx (\mathbf{a} \cdot \psi)^3$ we find that

$$\begin{aligned} \pi \dot{a}_j &= \langle \mathcal{F}'' (\mathbf{a} \cdot \psi) \chi | \phi_j^\dagger \rangle + \frac{1}{6} \langle \mathcal{F}''' (\mathbf{a} \cdot \psi)^3 | \phi_j^\dagger \rangle + \eta \langle \gamma'(S) (\mathbf{a} \cdot \psi) | \phi_j^\dagger \rangle \\ &\quad + \langle \mathbf{a} \cdot \nabla_{\mathbf{r}} \chi | \phi_j^\dagger \rangle. \end{aligned} \quad (7.74)$$

Introducing the complex amplitude $a = a_1 + i a_2$ gives us the Stuart-Landau equation

$$\dot{a} = a(M_1 |a|^2 + M_2 \eta), \quad (7.75)$$

where

$$\pi M_1 = \frac{1}{6} \langle \mathcal{F}''' \psi_1^3 | \phi_1^\dagger \rangle + \langle \mathcal{F}'' \psi_1 V_1^2 | \phi_1^\dagger \rangle + \langle \partial_{x_1} V_1 | \phi_1^\dagger \rangle, \quad (7.76)$$

$$\pi M_2 = \langle \mathcal{F}'' \psi_1 V_4 | \phi_1^\dagger \rangle + \langle \gamma'(S) \psi_1 | \phi_1^\dagger \rangle + \langle \partial_{x_1} V_4 | \phi_1^\dagger \rangle. \quad (7.77)$$

Hence, there is a pitchfork equation with branches of solutions $(a_1, a_2) = (0, 0)$ (a standing spot) and $|a|^2 = -M_2 \eta / M_1$ for $M_2 \eta / M_1 < 0$ and $M_{1,2} \neq 0$ (a travelling spot). Beyond a drift instability the speed of the travelling spot will scale as $\sqrt{|\eta M_2 / M_1|}$ for small η . Treating g as the bifurcation parameter we see that the speed scales as $\sqrt{g - 1/\alpha}$, which compares well with direct numerical simulations near the bifurcation point (not shown).

7.7 Scattering

For anatomical interactions which decay exponentially quickly, such as Mexican or wizard hat functions, then we would expect a neural field model with a single spot solution to also support multiple spots, at least for some large separation between spots. This then begs the question of how spots interact when they come close together. Interestingly it has already been found numerically that spots in a model with spike frequency adaptation can scatter like dissipative solitons [8]. Here we

adapt techniques originally developed by Ei et al. [10, 11], for multi-component reaction diffusion systems, to show that two slowly moving spots will reflect from each other in a head-on collision.

We introduce the sum of two spots with centers offset by a vector \mathbf{h} as

$$S(\mathbf{r}; \mathbf{h}) = S(\mathbf{r}) - S(\mathbf{r} - \mathbf{h}), \quad S(\mathbf{r}) = S(|\mathbf{r}|). \quad (7.78)$$

We then consider solutions of the form

$$X(\mathbf{r}, t) = \tau(\mathbf{p}) [S(\mathbf{r}; \mathbf{h}) + \mathbf{a} \cdot \psi(\mathbf{r}) + \mathbf{b} \cdot \psi(\mathbf{r} - \mathbf{h}) + \chi(\mathbf{r}, t)]. \quad (7.79)$$

We may then adapt the technique of Sect. 7.6, closely following [11], to derive the equations of motion for $(\mathbf{p}, \mathbf{h}, \mathbf{a}, \mathbf{b})$ as

$$\dot{\mathbf{p}} = \mathbf{a} + \mathbf{G}_1(\mathbf{h}), \quad (7.80)$$

$$\dot{\mathbf{h}} = \mathbf{b} - \mathbf{a} + \mathbf{G}_1(\mathbf{h}) - \mathbf{G}_2(\mathbf{h}), \quad (7.81)$$

$$\dot{\mathbf{a}} = \nabla W(\mathbf{a}) + \mathbf{H}_1(\mathbf{h}), \quad (7.82)$$

$$\dot{\mathbf{b}} = \nabla W(\mathbf{b}) + \mathbf{H}_2(\mathbf{h}), \quad (7.83)$$

where

$$\mathbf{G}_1(\mathbf{h}) = \begin{bmatrix} \langle \mathcal{F}(S(\cdot; \mathbf{h})) | \psi_1^\dagger \rangle \\ \langle \mathcal{F}(S(\cdot; \mathbf{h})) | \psi_2^\dagger \rangle \end{bmatrix} \quad \mathbf{G}_2(\mathbf{h}) = \begin{bmatrix} \langle \mathcal{F}(S(\cdot + \mathbf{h}; \mathbf{h})) | \psi_1^\dagger \rangle \\ \langle \mathcal{F}(S(\cdot + \mathbf{h}; \mathbf{h})) | \psi_2^\dagger \rangle \end{bmatrix}, \quad (7.84)$$

$$\mathbf{H}_1(\mathbf{h}) = \begin{bmatrix} \langle \mathcal{F}(S(\cdot; \mathbf{h})) | \phi_1^\dagger \rangle \\ \langle \mathcal{F}(S(\cdot; \mathbf{h})) | \phi_2^\dagger \rangle \end{bmatrix} \quad \mathbf{H}_2(\mathbf{h}) = \begin{bmatrix} \langle \mathcal{F}(S(\cdot + \mathbf{h}; \mathbf{h})) | \phi_1^\dagger \rangle \\ \langle \mathcal{F}(S(\cdot + \mathbf{h}; \mathbf{h})) | \phi_2^\dagger \rangle \end{bmatrix}, \quad (7.85)$$

and

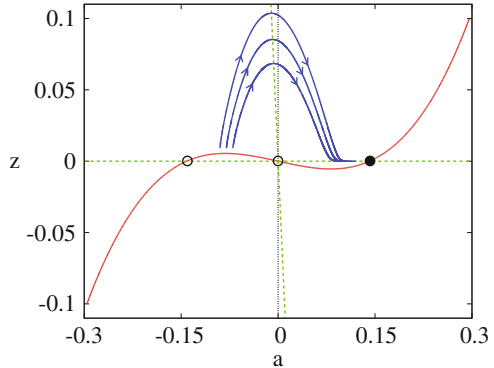
$$W(\mathbf{x}) = \frac{1}{4}M_1|\mathbf{x}|^4 + \frac{1}{2}\eta M_2|\mathbf{x}|^2. \quad (7.86)$$

Now for a spot shape like that of (7.23) we may use the asymptotic properties of $K_0(r)$ to see that $q(r) \sim \exp(-r)/\sqrt{r}$ for large r . We expect similar decay properties of spots in the case of steep sigmoidal firing rates. In this case we can use results from [11], valid as $h = |\mathbf{h}| \rightarrow \infty$, to represent the interaction functions in the form

$$G_i(\mathbf{h}) = (-1)^{i-1} G_0 \frac{1}{\sqrt{h}} e^{-h} \mathbf{e}, \quad H_i(\mathbf{h}) = (-1)^{i-1} H_0 \frac{1}{\sqrt{h}} e^{-h} \mathbf{e}, \quad \mathbf{e} = \frac{\mathbf{h}}{h}, \quad (7.87)$$

for constants G_0 and H_0 , which we shall assume to be positive.

Fig. 7.9 Phase plane for the dynamical system (7.89), showing nullclines and some typical trajectories. The consequence for spot-spot interactions is that for small η then slowly moving spots will scatter from each other by reflection. Parameters are $\eta = M_2 = G_0 = H_0 = 0.1$ and $M_2 = -0.5$



Now consider the interaction of two travelling pulses, with one centred at \mathbf{p} and another at $-\mathbf{p}$ moving on a line joining their centres so that the separation between them is $\mathbf{h} = 2\mathbf{p}$. For simplicity we shall take \mathbf{p} to be along the x_1 axis and write $\mathbf{p} = p(1, 0)$ and set $\mathbf{a} = a(1, 0)$. In this case we have that

$$\dot{p} = a + G_0 f(p), \quad \dot{a} = M_1 a^3 + M_2 a \eta + H_0 f(p), \quad (7.88)$$

where $f(p) = e^{-2p}/\sqrt{2p}$. Introducing $z = f(p)$ we may rewrite this dynamical system as

$$\dot{z} = -2zQ(z)[a + G_0 z], \quad \dot{a} = H_0 z - f(a), \quad (7.89)$$

where $Q(z) = 1 + (4f^{-1}(z))^{-1} > 0$ and $f(a) = -M_1 a^3 - M_2 a \eta$. There are stationary solutions of (7.89) in the (a, z) plane at $(v_-, 0)$, $(0, 0)$, and $(v_+, 0)$, where $v_{\pm} = \pm \sqrt{-M_2 \eta / M_1}$ (with $M_1 < 0$ and $M_2 \eta > 0$). Linear stability analysis around a stationary solution gives a pair of eigenvalues that determine stability in the form $\lambda_1 = -2a$ and $\lambda_2 = -f'(a)$. Hence the only stable solution is $(v_+, 0)$. An analysis of the phase plane, see Fig. 7.9, shows that trajectories that start with $a < 0$ and small z (namely spots moving with negative velocity toward each other from far apart) ultimately move to $a = v_+ > 0$ with small z so that the spots reverse their motion and travel with positive velocity away from each other. Hence we expect two travelling spots to reflect from each other, as shown in a simulation of the full model in Fig. 7.10.

7.8 Discussion

In this chapter we have shown how to analyse the properties of spots in planar neural field models with spike frequency adaptation, using a mixture of techniques ranging from direct numerical simulations, through amplitude equations to explicit results

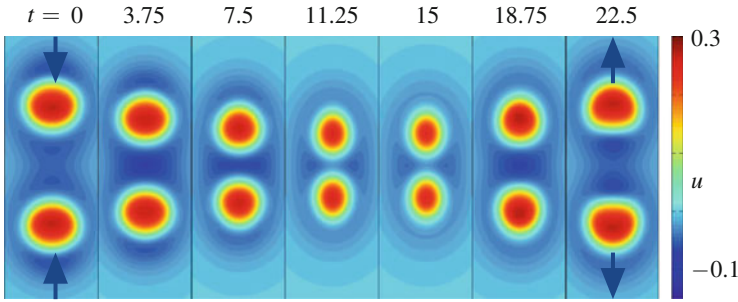


Fig. 7.10 Results of a direct numerical simulation of two scattering spots in the neural field model with Heaviside firing rate and parameters $\gamma = 4$, $\mu = 0.5$, $g = 0.5$ and $\alpha = 5$. The overall spatial domain has a size of 51.2×51.2 of which we see a zoomed set of seven snapshots at indicated times

for the special case of a Heaviside firing rate function using an interface approach. There are a number of natural extensions of this work that may be developed. The scattering theory that we developed is valid only for slowly moving spots, which is expected to be the case when model parameters are near to that defining the onset of a drift instability for a single spot. However, numerical simulations show that fast moving spots may scatter differently to slow moving ones, with the possibility of *fusion* and *annihilation*, as well as repulsion. In this case it is likely that these more complicated scenarios can be understood using the scatter theory of Nishiura et al. [22]. In this framework the scattering process is understood in terms of the stable and unstable manifolds of a certain unstable pattern that has the form of a two-lobed *peanut* shape. These solutions are expected to arise via a symmetry breaking bifurcation of spots to solutions with D_2 symmetry (generated by rotations of π , and reflection across a central axis). The computation of the scatter requires the numerical calculation of non-rotationally symmetric solutions, and the numerical schemes for PDEs that we have described here are easily generalised. Moreover, for the Heaviside firing rate we can use a formulation in [8] to express such solutions purely as line integrals, with a substantial reduction in dimensionality that will facilitate an exhaustive numerical bifurcation analysis. The interaction of drift and peanut modes of instability is known to generate a rotational motion of travelling spots, at least in three component reaction diffusion equations [26]. It should also be possible to extend the center manifold reduction developed here to describe the behaviour of localised solutions in the neighbourhood of such a co-dimension two bifurcation point. Finally, we flag up the utility of the interface approach in two spatial dimensions for analysing not only localised states, but extended solutions such as spirals [20]. All of the above are topics of ongoing research and will be reported upon elsewhere.

Acknowledgements The authors would like to acknowledge useful discussions with Paul Bressloff, Grégory Faye, Carlo Laing and David Lloyd that have helped to improve the presentation of the ideas in this chapter.

Appendix

To establish that ϕ^\dagger can be written as a linear transformation of ϕ we proceed by writing $M = P \text{diag}(\lambda_+, \lambda_-) P^{-1}$, where $P = [v_+ \ v_-]$, and v_\pm are the right eigenvectors of M :

$$v_\pm = \begin{bmatrix} \alpha g \\ -(\alpha + \lambda_\pm) \end{bmatrix}, \quad (7.90)$$

with

$$\lambda_\pm = \frac{-(1 + \alpha) \pm \sqrt{(1 - \alpha)^2 - 4\alpha g}}{2}. \quad (7.91)$$

In this case we may recast the eigenvalue problem $\mathcal{L}\phi = \lambda\phi$ as

$$\begin{bmatrix} \lambda_+ & 0 \\ 0 & \lambda_- \end{bmatrix} P^{-1}\phi + \alpha w \otimes f'(q) P^{-1} \begin{bmatrix} 1 & 0 \\ 0 & 0 \end{bmatrix} \phi = \lambda P^{-1}\phi. \quad (7.92)$$

Similarly we may write $M^\dagger = R \text{diag}(\lambda_+, \lambda_-) R^{-1}$, where $R = [w_+ \ w_-]$, and w_\pm are the right eigenvectors of M^\dagger :

$$w_\pm = \begin{bmatrix} 1 \\ \alpha + \lambda_\pm \end{bmatrix}. \quad (7.93)$$

The adjoint operator \mathcal{L}^\dagger can be found as

$$\mathcal{L}^\dagger = M^\dagger + \alpha f'(q) w \otimes \begin{bmatrix} 1 & 0 \\ 0 & 0 \end{bmatrix}. \quad (7.94)$$

By inspection it can be seen that the adjoint equation $\mathcal{L}^\dagger \phi^\dagger = \bar{\lambda} \phi^\dagger$ has a solution

$$\phi^\dagger = f'(q) R P^{-1} \bar{\phi}, \quad (7.95)$$

which can be evaluated to give (7.53). Here we make use of the result that

$$P R^{-1} \begin{bmatrix} 1 & 0 \\ 0 & 0 \end{bmatrix} R P^{-1} = \begin{bmatrix} 1 & 0 \\ 0 & 0 \end{bmatrix}. \quad (7.96)$$

References

1. Amari, S.: Dynamics of pattern formation in lateral-inhibition type neural fields. *Biol. Cybern.* **27**, 77–87 (1977)
2. Avitabile, D.: Computation of planar patterns and their stability. PhD thesis, Department of Mathematics, University of Surrey (2008)
3. Blomquist, P., Wyller, J., Einevoll, G.T.: Localized activity patterns in two-population neuronal networks. *Physica D* **206**, 180–212 (2005)
4. Bressloff, P.C., Kilpatrick, Z.P.: Two-dimensional bumps in piecewise smooth neural fields with synaptic depression. *SIAM J. Appl. Math.* **71**, 379–408 (2011)
5. Coombes, S.: Waves, bumps, and patterns in neural field theories. *Biol. Cybern.* **93**, 91–108 (2005)
6. Coombes, S., Owen, M.R.: Exotic dynamics in a firing rate model of neural tissue with threshold accommodation. *AMS Contemp. Math. Fluids Waves: Recent Trends Appl. Anal.* **440**, 123–144 (2007)
7. Coombes, S., Venkov, N.A., Shiau, L., Bojak, I., Liley, D.T.J., Laing, C.R.: Modeling electrocortical activity through improved local approximations of integral neural field equations. *Phys. Rev. E* **76**, 051901 (2007)
8. Coombes, S., Schmidt, H., Bojak, I.: Interface dynamics in planar neural field models. *J. Math. Neurosci.* **2**(1), 9 (2012)
9. Doedel, E., Oldeman, B.: Auto-07p: continuation and bifurcation software for ordinary differential equations. Technical report, Concordia University, Montreal (2009)
10. Ei, S.-I., Mimura, M., Nagayama, M.: Pulse–pulse interaction in reaction–diffusion systems. *Physica D* **165**, 176–198 (2002)
11. Ei, S.-I., Mimura, M., Nagayama, M.: Interacting spots in reaction diffusion systems. *Discret. Contin. Dyn. Syst. Ser. A* **14**, 31–62 (2006)
12. Ermentrout, G.B.: Neural nets as spatio-temporal pattern forming systems. *Rep. Prog. Phys.* **61**, 353–430 (1998)
13. Faye, G., Rankin, J., Chossat, P.: Localized states in an unbounded neural field equation with smooth firing rate function: a multi-parameter analysis. *J. Math. Biol.* **66**(6), 1303–1338. doi:10.1007/s00285-012-0532-y
14. Foliás, S.E.: Nonlinear analysis of breathing pulses in a synaptically coupled neural network. *SIAM J. Appl. Dyn. Syst.* **10**, 744–787 (2011)
15. Foliás, S.E., Bressloff, P.C.: Breathing pulses in an excitatory neural network. *SIAM J. Appl. Dyn. Syst.* **3**(3), 378–407 (2004)
16. Foliás, S.E., Bressloff, P.C.: Breathers in two-dimensional neural media. *Phys. Rev. Lett.* **95**, 208107(1–4) (2005)
17. Goldman-Rakic, P.S.: Cellular basis of working memory. *Neuron* **14**, 477–485, (1995)
18. Gurevich, S.V., Amiranashvili, Sh., Purwins, H.-G.: Breathing dissipative solitons in three-component reaction-diffusion systems. *Phys. Rev. E* **74**, 066201(1–7) (2006)
19. Kilpatrick, Z.P., Bressloff, P.C.: Effects of synaptic depression and adaptation on spatiotemporal dynamics of an excitatory neuronal network. *Physica D* **239**, 547–560 (2010)
20. Laing, C.R.: Spiral waves in nonlocal equations. *SIAM J. Appl. Dyn. Syst.* **4**, 588–606 (2004)
21. Laing, C.R., Troy, W.C.: PDE methods for nonlocal models. *SIAM J. Appl. Dyn. Syst.* **2**, 487–516 (2003)
22. Nishiura, Y., Teramoto, T., Ueda, K.-I.: Scattering of traveling spots in dissipative systems. *Chaos* **15**, 047509(1–10) (2005)
23. Owen, M.R., Laing, C.R., Coombes, S.: Bumps and rings in a two-dimensional neural field: splitting and rotational instabilities. *New J. Phys.* **9**, 378 (2007)
24. Pinto, D.J., Ermentrout, G.B.: Spatially structured activity in synaptically coupled neuronal networks: II. Lateral inhibition and standing pulses. *SIAM J. Appl. Math.* **62**, 226–243 (2001)

25. Sandstede, B., Scheel, A.: Defects in oscillatory media: toward a classification. *Dyn. Syst.* **3**, 1–68 (2004)
26. Teramoto, T., Suzuki, K., Nishiura, Y.: Rotational motion of traveling spots in dissipative systems. *Phys. Rev. E* **80**, 046208(1–10) (2009)